Available online at www.sciencedirect.com
SCIENCE DIRECT
Journal of Non-Crystalline Solids 352 (2006) 646–656
JOURNAL OF NON-CRYSTALLINE SOLIDS
www.elsevier.com/locate/jnoncrysol

Nanofabrication in transparent materials with a femtosecond pulse laser

Yasuhiko Shimotsuma [a,*], Kazuyuki Hirao [a], Jianrong Qiu [b,c], Kiyotaka Miura [b,d]

[a] Department of Material Chemistry, Graduate School of Engineering, Kyoto University, Kyotodaigaku-Katsura, Nishikyo-ku, Kyoto 615-8510, Japan
[b] Japan Science and Technology Agency, Keihanna-Plaza, Kyoto 619-0237, Japan
[c] Department of Materials Science and Engineering, Zhejiang University, 38 Zheda Road, Hangzhou 310027, China
[d] Optical Device Development Department, Central Glass Corporation, 5253 Okiube, Ube, Yamaguchi 755-0001, Japan

Available online 3 March 2006

Abstract

Femtosecond lasers have been applied for materials processing when high accuracy and small structure size are required. Various induced structures have been observed inside glasses after the femtosecond laser irradiation. We report the femtosecond laser induced refractive-index change, space-selective valence state change of active ions, formation of nanograting, and precipitation and distribution of nanoparticles. We systematically studied the morphology of structures that are induced in the bulk of transparent materials by the tightly focused femtosecond laser radiation. Rugby-ball-like asymmetric induced structures were observed inside Ag^{+}-doped silicate glass. These structures are due to the aggregation of Ag nanoparticles at the depth of the focal point. The size of the induced structure depended on the time interval between successive femtosecond laser pulses. In the case of zinc-tellurite glass, TeO_2 rich parts were formed in the center of the focal spot, while zinc migrated to the outside. The mechanisms of the observed phenomena are discussed.

Keywords: Laser–matter interactions; Optical microscopy; Scanning electron microscopy; Silica; Silicates; Soda–lime–silica; Tellurites

1. Introduction

Femtosecond lasers have been used as a powerful tool to clarify elementary processes, such as excitation-energy relaxation and both electron and proton transfer on nanosecond and picosecond time scales that occur in a micrometer-sized area. In the past decades, femtosecond lasers have been widely used in micro processing. The femtosecond laser has two apparent features compared with CW and long pulsed lasers: (1) elimination of the thermal effect due to extremely short energy deposition time and (2) participation of various non-linear processes enabled by high localization of laser photons in both time and spatial domains. Due to the ultrashort light–matter interaction time and the high peak power density, material processing with the femtosecond laser is generally characterized by the absence of heat diffusion and consequently molten layers [1]. The photoinduced reactions are expected to occur only near the focused part of the laser beam due to multiphoton processes. In the past several years, many research efforts have been devoted to the field of three-dimensional microscopic modifications to transparent materials using femtosecond lasers. Promising applications have been demonstrated for the formation of three-dimensional optical memories [2,3] and multicolor images [4], the direct writing of optical waveguides [5,6], waveguide couplers and splitters [7,8], waveguide optical amplifiers [9], and optical gratings [10,11]. Furthermore, in the recent applied researches, femtosecond lasers have been used as a fabrication tool of photonic crystals [12,13]. To micromachine a transparent material in three-dimensions, a femtosecond laser beam is tightly focused into the bulk of the material. High laser intensity in the focal volume

* Corresponding author. Tel.: +81 75 383 2418; fax: +81 75 383 2410.
E-mail address: yshimo@collon1.kuic.kyoto-u.ac.jp (Y. Shimotsuma).

0022-3093/$ - see front matter © 2006 Elsevier B.V. All rights reserved.
doi:10.1016/j.jnoncrysol.2005.11.060

induces non-linear absorption of the laser energy by the material via multiphoton, tunneling, and avalanche ionization [14,15]. If sufficient laser energy is deposited, permanent structural changes are produced inside a material at the location of the laser focus. Depending on laser, focusing, and material parameters, different mechanisms may play a role in producing the structural changes and lead to different morphologies from small density and refractive-index modification, to the generation of color centers, and to the formation of voids [16]. Although the process of energy absorption is now well understood [17], little is known about the actual structural change in the focal spot [18–20]. Furthermore, although an ablation threshold and morphology of damaged surface by the femtosecond laser irradiation on the material surface have been investigate in detail [21,22], there are few morphological analyses of the induced structure inside transparent materials [23,24].

In this paper, we present a systematic study of the morphology of the induced structure in the bulk of Ag^+-doped silicate glass, fused silica glass, and tellurite glass by the tightly focused femtosecond laser radiation. Due to the aggregation of Ag nanoparticles at the depth of the focal point, rugby-ball-like asymmetric induced structures were observed inside Ag^+-doped silicate glass. Due to the difference of the thermal diffusivity of materials, we confirmed that there was a relation between the size of induced structure and the time interval between successive femtosecond laser pulses. In the case of zinc-tellurite glass, we confirmed by means of an electron probe microanalysis (EPMA) that TeO_2 rich parts were formed in the center of a focal spot, while zinc migrated to the outside. Moreover, we observed that the length of the induced structure is variable depending on the depth of the focal spot location from sample surface. From the comparison of tellurite glass with fused silica glass, we also found differences in the length of the induced structure depending on the linear and non-linear optical properties. The length of the induced structure depends on the pulse energy of the femtosecond laser irradiation. Moreover, we observed the emergence of self-organized periodic structures of nanometer size inside fused silica glass and tellurium dioxide single crystal after irradiation by an intense femtosecond laser single beam [19,20]. The phenomenon is interpreted in terms of interference between the incident light field and the electric field of a bulk electron plasma wave, resulting in periodic modulation of the electron plasma concentration and permanent structural changes in glass. The observed phenomena are useful in the fabrication of three-dimensional symmetric micro and nanostructures of many monolithic photonic devices and microelectromechanical system applications.

2. Experimental

2.1. Glass preparation

Typical Ag^+-doped silicate, zinc-tellurite, and niobium-tellurite glasses were prepared in this experiment. Reagent grade SiO_2, $CaCO_3$, Na_2CO_3, Ag_2O, ZnO, Nb_2O_5, and TeO_2 were used as starting materials. A mixed batch of ~20 g was melted under an ambient atmosphere. Glass samples were obtained by quenching the melt to room temperature. The resultant transparent glass samples were cut, polished, and subjected to experiments. To compare materials, we also used tellurium dioxide single crystal (tetragonal crystal, space group: $P4_12_12$), TeO_2 single crystal (Oxide Corp., z-cut with orientation of (0, 0, 1)) and fused silica glass, ED-C (Tosoh Quartz Corp., brands of wet silica with OH < 1 ppm) in this experiment. The glass compositions prepared in the experiments are shown in Table 1.

Table 1
Compositions of glasses prepared in this study (mol%)

Sample	SiO_2	CaO	Na_2O	Ag_2O	ZnO	TeO_2	Nb_2O_5	TeO_2
AG	70	10	20	0.1				
ZN					20	80		
NB							15	85

2.2. Femtosecond-laser irradiation and characterization

A regeneratively amplified 800 nm Ti:Sapphire laser that emits 120 fs, mode-locked pulses was used. The laser beam was focused by a 100× objective lens with a numerical aperture of 0.95 into the interior of the glass sample with the help of an XYZ stage. In order to clarify the effect of thermal diffusion on the morphology of the induced structure, we used a femtosecond laser beam with repetition rate of 1 kHz or 200 kHz and kept the total irradiation energy constant. Furthermore, the position of the focal spot was changed from 20 μm to 200 μm beneath the glass surface. Using optical microscopy, we observed the shape of the induced structure in the glass samples. After the femtosecond laser irradiation, the glass samples were polished to the depth of the beam waist location. The polished sample surfaces were analyzed by electron probe microanalyzer (EPMA, JEOL JXA-8900-RL), scanning electron microscope (SEM, JEOL, model JSM-6700F), Auger electron spectroscopy (AES, PHI, model SAM-680), and Raman spectroscopy (Tokyo Instruments Inc. Nanofinder 10). All of the experiments were carried out at room temperature. The absorption spectra of samples were measured with a spectrophotometer (JASCO V-570), and absorbance of all the samples at the wavelength of 800 nm was lower than 0.1.

3. Results

3.1. Ag nanoparticle formation without annealing process

After irradiation by the focused femtosecond laser with pulse energy of 1.0 μJ on each spot for 1 s (i.e. 2×10^5 pulses), a 10 μm spot was formed in the focused area of the laser beam in the Ag^+-doped silicate glass sample. Fig. 1 shows optical microscope images of the top and side

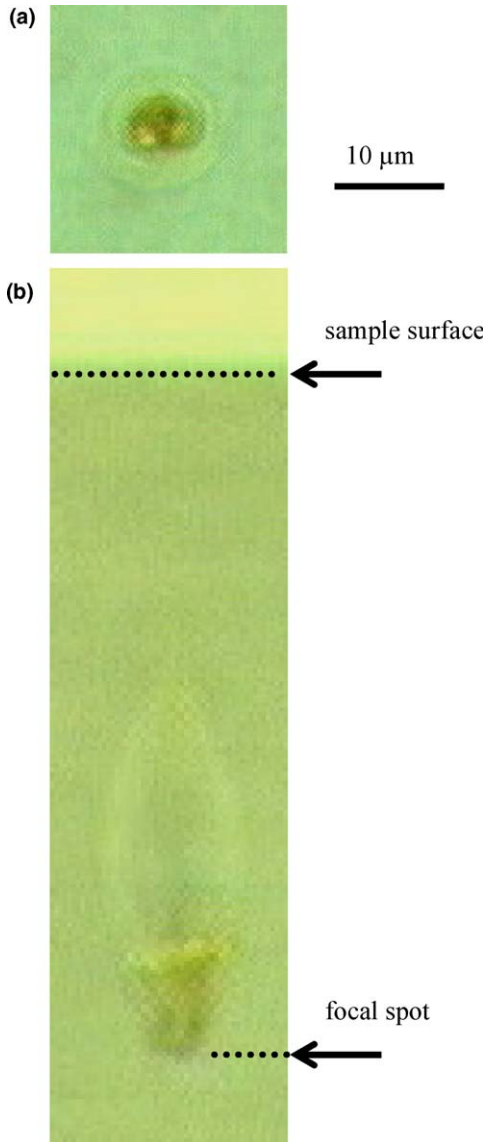

Fig. 1. Optical microscope images of an induced structure inside Ag^{+}-doped silicate glass by the irradiation of 1.0 μJ, 120 fs laser pulses at a 200 kHz repetition rate (a: top view, b: side view). The pulses were focused by a 0.95-NA microscope objective.

view of a focal spot location. A yellow-colored area with a diameter of about 6 μm was observed at the center of the focal spot, while rugby-ball-like asymmetric structure with the length of about 36 μm was observed in the side view of glass sample. Although no apparent structurally changed area was observed below the focal spot, refractive-index changed area could be observed above the focal point depth (Fig. 1(b)). In addition, a yellow-colored area was observed in the region of about 10 μm upper part from a focal spot. In the case of the repetition rate of 1 kHz, the area near the focal spot became gray after the femtosecond laser irradiation and yellow after further annealing at 550 °C for 10 min [25,26]. Qiu et al. suggested that the yellow-colored area indicates the formation of Ag nanoparticles due to the aggregation of Ag atoms [25]. To test the formation of Ag nanoparticles without annealing process, we carried out the elemental analysis on the polished sample surface to the depth of the focal spot by EPMA (Fig. 2(b)). Fig. 3 shows Raman spectra of the Ag^{+}-doped glass sample before and after femtosecond laser irradiation. Excitation wavelength is 488 nm. There was an apparent increase in the fluorescence in the wavelength region from 520 to 680 nm in the irradiated region. We carried out the Raman spectrum mapping using peak at 590 nm, which was attributed to the emission of silver nanoparticle [27]. Fig. 4 indicates that the optical microscope image and the Raman spectrum mapping after the femtosecond laser irradiation are in a good agreement.

3.2. Thermal accumulation due to the irradiation of laser with high repetition rate

Fig. 5 shows optical microscope images of induced structures by 0.8 μJ laser pulses (i.e. laser intensity $\sim 8.0 \times 10^{14}$ W/cm^2) inside various materials. The total irradiation energy was 0.8 mJ for 1000 pulses at 1 kHz and 1.28 mJ for 1600 pulses at 200 kHz, respectively. Although the size of the induced structures inside TeO_2 single crystal and fused silica glass were almost the same (2–3 μm) at different repetition rate, in the case of zinc-tellurite glass,

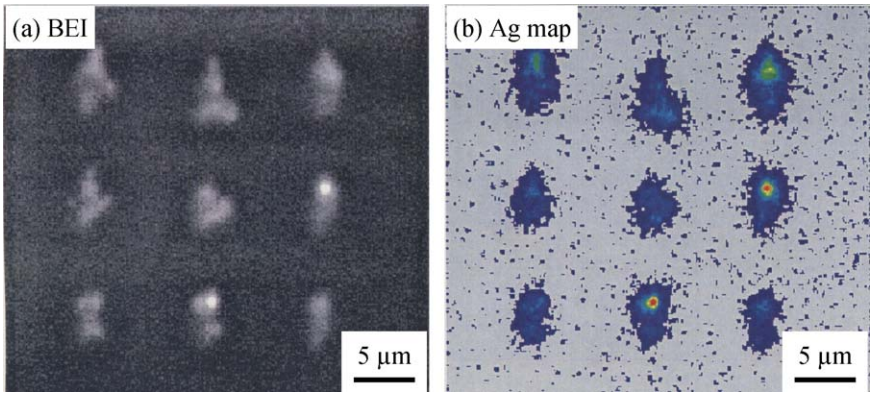

Fig. 2. Backscattering electron image (a) and Ag spectrum mapping image (b) on the polished sample surface to the depth of focal spot for Ag^{+}-doped silicate glass.

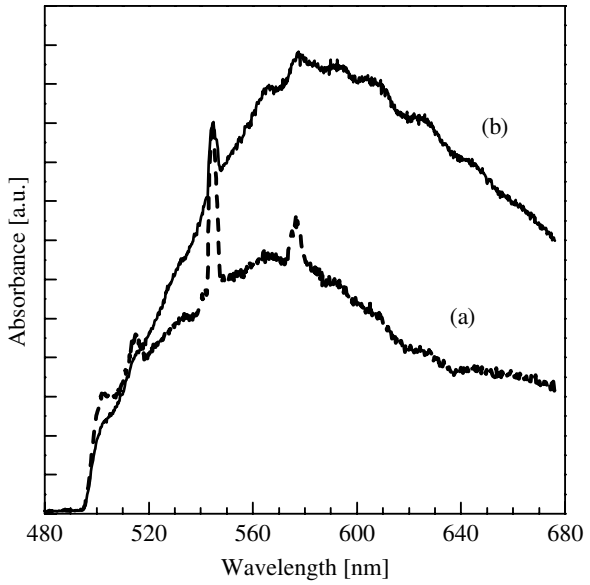

Fig. 3. Raman spectra of the Ag^{+}-doped silicate glass before (a: dashed line) and after (b: solid line) femtosecond laser irradiation. Excitation wavelength is 488 nm.

a cracked structure (~3 μm) and a large concentric ring structure (~18 μm) were induced at 1 kHz and 200 kHz, respectively. Several rings, indicating regions of different refractive index, were visible in Fig. 5(b). Comparing the structures induced by the two different repetition rates, it is apparent that the induced structures depend on the thermal diffusion during the time interval between successive pulses.

Fig. 6 shows the dependence of the diameter of an induced structure inside zinc-tellurite glass on the number of pulses during irradiation with 1.0 μJ femtosecond laser pulses at 200 kHz repetition rate. The dashed line shows a fitted curve of the experimental data. The diameter of the structures, D increases approximately as one-half power of the number of incident laser pulses, N_p ($D \propto -\sqrt{1/N_p}$). The diameter saturates at ~20 μm after ~10^5 pulses, most likely because the structure itself distorts the focus enough to lower the laser intensity below the breakdown threshold, thereby preventing further energy deposition. Similar thermal accumulation effects have been seen inside the fused silica by means of high repetition rate, ultrashort pulse trains [28]. On the other hand, since the thermal diffusivity of TeO_2 single crystal and fused silica glass is larger than one of zinc-tellurite glass, thermal accumulation is smaller. Consequently, the size of induced structures inside TeO_2 single crystal and fused silica glass are almost the same at different repetition rates.

To measure the movement of elements in the focal volume due to the thermal accumulation by the high repetition rate irradiation, we carried out spectral mapping of the elements on the polished sample surface using EPMA. Fig. 7 shows the backscattering electron image (BEI) and the spectral mapping of the elements constituting the surface. The BEI reveals bright regions with high density of material in the center of the structurally changed area. An oxygen mapping indicates that the oxygen concentration does not change after the femtosecond laser irradiation. On the other hand, zinc and tellurium mapping indicate that the concentrations of zinc and tellurium in the center region decrease and increase, respectively.

3.3. Polarization-dependent self-organized nanostructure formation

We previously observed the anomalous anisotropic light scattering in Ge-doped silica glass and rare-earth-ion-doped fluoroaluminate glass [18,29]. This observed phenomenon was considered to be due to the angular distribution of photoelectrons along laser polarization and the light scattering of the polarization-dependent permanent microstructure induced by the polarized femtosecond laser itself. Fig. 8 shows the secondary electron images (SEI) of the polished sample surface of fused silica glass and TeO_2 single crystal. In addition, BEI of the same surface of fused silica glass is shown in Fig. 9. It is well known that the SEI reveals the surface morphology, while the BEI is sensitive to the atomic weight of the elements or the density of material

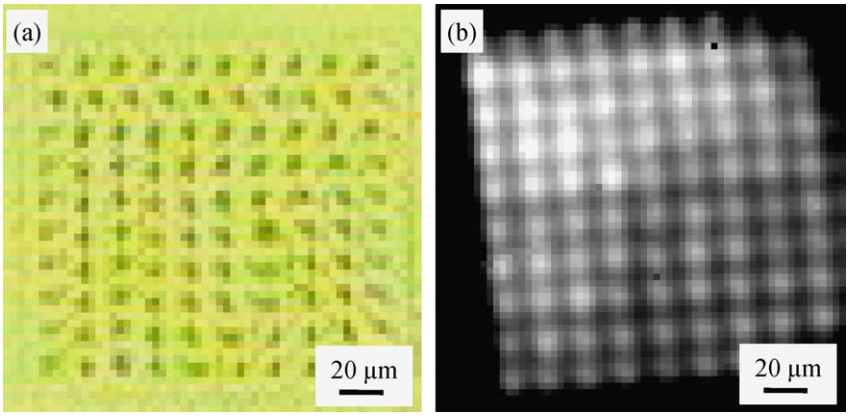

Fig. 4. Optical microscope image (a) and Raman spectrum mapping using a peak intensity at 590 nm (b) of the induced structure inside the Ag^{+}-doped silicate glass after the femtosecond laser irradiation at 200 kHz. Note that the excitation wavelength in the Raman measurement is 488 nm.

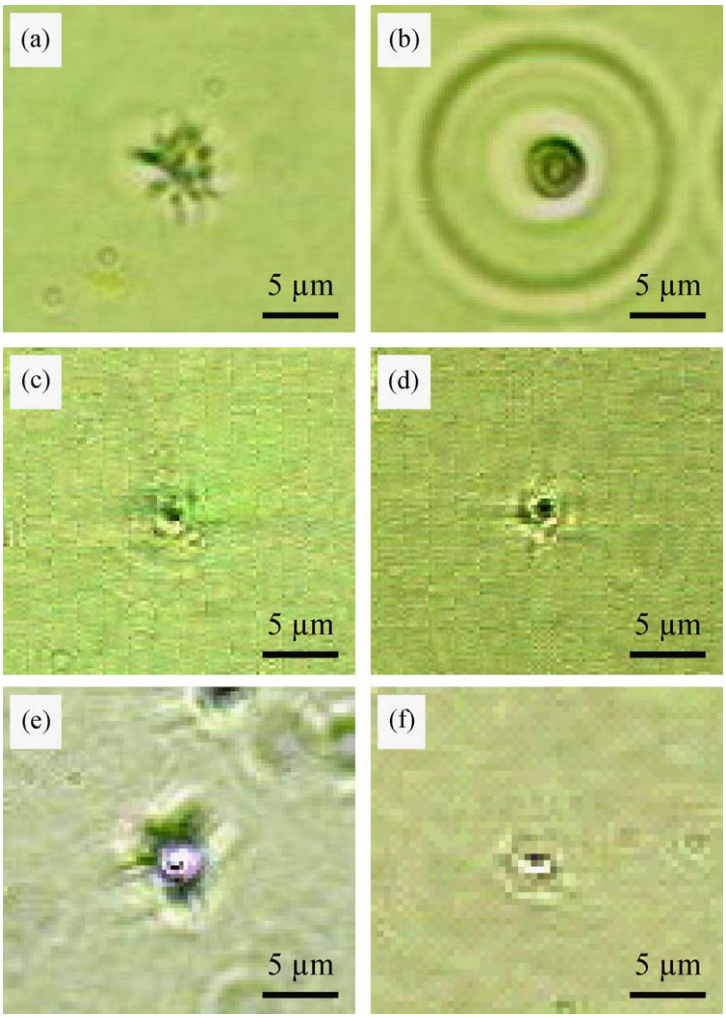

Fig. 5. Optical microscope images of induced structure by 0.8 μJ laser pulses inside zinc-tellurite glass (a), (b), TeO_2 single crystal (c), (d), and fused silica glass (e), (f), respectively. (a), (c), (e) the irradiation time is 1 s (i.e. 1000 pulses) at 1 kHz and (b), (d), (f) the irradiation time is 1/125 s (i.e. 1600 pulses) at 200 kHz repetition rate, respectively.

constituting the observed surface. The SEI of the polished fused silica glass sample surface indicates that the morphology in the focal spot dose not change, namely, a void does not exist [19]. On the other hand, in the case of TeO_2 single crystal, stripe-like voids with the nanoscale pitch and width exist within the focal spot [20]. The SEI of TeO_2 single crystal shows that the periodic voids of ~30 nm width are aligned perpendicular to the polarization direction of the laser beam. Furthermore, in common with the SEI of TeO_2 single crystal, the BEI of fused silica glass shows a periodic structure of stripe-like dark regions of material with low density and of ~20 nm width, which are aligned perpendicular to the laser polarization direction. Furthermore, in the experiment of fused silica glass, we observed the decrease of the grating period with an increase of the exposure time. When the pulse energy was 1 μJ, the grating periods were about 240 nm, 180 nm and 140 nm for the number of light pulses of 5×10^4, 20×10^4 and 80×10^4, respectively. A pulse energy of 1 μJ corresponds to an intensity of about 2×10^{14} W/cm^2 in our experiments. This indicates a logarithmic dependence of the grating period Λ on the number of light pulses N_{pulse} [20]. The dependence of the observed periodic nanostructures on pulse energy for a fixed exposure time was also investigated, and an increase of the period with the pulse energy was observed. For the number of light pulses of 20×10^4, grating periods of 180 nm, 240 nm and 320 nm were measured at pulse energies of 1 μJ, 2 μJ and 2.8 μJ, respectively [19].

3.4. Size control with the laser irradiation conditions

We observed the side view of an induced structure by 1.0 μJ laser pulses on each spot for 1 s (i.e. 2×10^5 pulses) inside niobium-tellurite glass and fused silica glass using optical microscope. In the case of niobium-tellurite glass, the length of the induced structure was elongated along the laser propagation direction when deepening the focal spot location (Fig. 10(a)). On the other hand, in the case of fused silica glass, the length was saturated at about

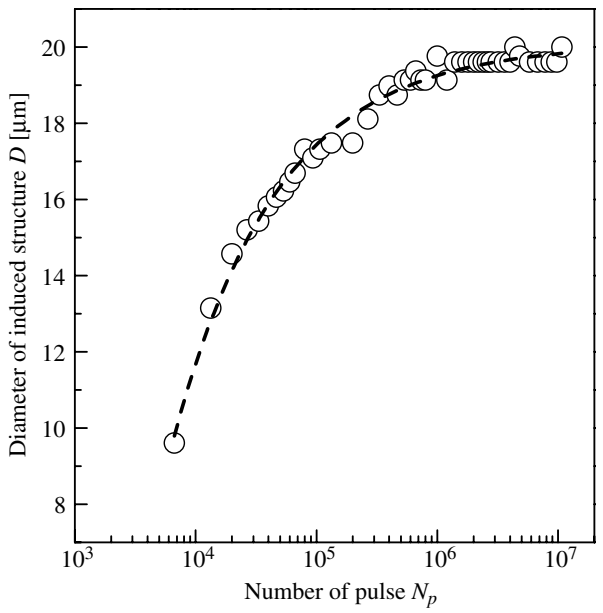

Fig. 6. Number of pulse dependence of the diameter of an induced structure inside zinc-tellurite glass during the 1.0 μJ laser pulses irradiation at 200 kHz repetition rate. The dashed line shows a fit of the −1-s power to the data.

30 μm in various focal spot depths (Fig. 10(b)). Fig. 11 shows the dependence of the length of the induced structure on the various focal spot depths. We also observed that the length of the induced structure is dependent on the pulse energy. Fig. 12 shows the pulse energy dependence of the length of induced structure at the focal spot depth of 60 μm in a niobium-tellurite glass. From these dependences, in the case of niobium-tellurite glass, the length of induced structure varies with the focal spot depth and pulse energy.

4. Discussion

4.1. Asymmetric induced structure formation

The BEI in Fig. 2 indicates that a high-density material constitutes the bright regions. Namely, the concentration of silver element is increased in the center of the focal spot in the case of Ag^+-doped silicate glass (Fig. 2(b)). We speculate that in the case of high repetition rate, Ag atoms are aggregated to form Ag nanoparticles without annealing process due to the shorter interval between successive pulses (Figs. 3 and 4). This difference of induced structure with the increase of repetition rate is concerned with thermal effect. In the case of 200 kHz repetition rate, the heat caused by the laser energy absorption was diffused ~1.9 μm during the time interval between successive pulses (5 μs). On the other hand, in the case of 1 kHz (interval of pulses: 1 ms), the heat could diffuse away out of focal volume to ~27 μm during the interval of successive pulses. Note that with the thermal diffusivity of the Ag^+-doped silicate glass sample $\alpha = 3.6 \times 10^{-7}$ m^2/s, the thermal diffusion length $\mu = \sqrt{2\kappa/\rho C_p R_R}$, κ is the thermal conductivity, C_p is the specific heat, ρ is the density, and R_R is the repetition rate of the irradiation laser pulse. From these results, when repetition rate is sufficiently high, an accumulation of heat is large; Ag atoms can be aggregated to form nanoparticles in the center of the focal spot without annealing process. Due to the scattering or reflection of laser beam with the Ag nanoparticle formation at the focal spot, a refractive-index change is only induced in the region toward the laser incidence. Finally, rugby-ball-like asymmetric structures are formed inside the Ag^+-doped silicate glass (Fig. 1). Our observations indicates that the femtosecond laser at a high repetition rate acts as a point source of heat inside the bulk of the material, and the morphology of the induced structure is dominated by the heat accumulation and radiation during the interval of successive pulses.

4.2. Thermal diffusion dependence on induced structure

As seen from Fig. 5, in the case of zinc-tellurite glass, the time interval between successive laser pulses at 200 kHz is much shorter than the time scale for thermal diffusion out of the focal volume, since the thermal diffusivity in zinc-tellurite glass is lower than in other materials. The thermal diffusivity of zinc-tellurite glass, TeO_2 single crystal, and fused silica glass is about 5.2×10^{-7} m^2/s, 1.3×10^{-6} m^2/s, and 1.2×10^{-6} m^2/s, respectively. As a result, successive laser pulses deposit energy faster than it can diffuse away, raising the temperature of the material in the focal spot. On a longer time scale, the heat deposited by successive pulses diffuses around the focal volume and melts a region much larger than the focal volume. An area surrounding the focal spot inside zinc-tellurite glass has been melted and resolidified non-uniformly resulting in the formation of numerous concentric rings with different optical constants (Fig. 5(b)). Similarly, zinc element diffuses away from the center of the focal volume, then zinc defects are formed (Fig. 7(d)), while tellurium element aggregates into the focal volume corresponding to the bright region of BEI (Fig. 7(c)). On the other hand, the spatial distribution of oxygen element does not change after the femtosecond laser irradiation (Fig. 7(b)). Cracks (diameter ~ 23 μm) around the circumference of the focal spot were observed in the BEI (Fig. 7). We assumed that these cracks formation could be explained by a surface relief created in the polishing process due to the density variations around the focal spot. Nukui et al. observed the structural change of ZnO–TeO_2 glass at high temperatures and they confirmed that the α-TeO_2 and $Zn_2Te_3O_8$ phases crystallized at high temperatures (~900 °C) in a ZnO–TeO_2 glass [30]. From these results, we assumed that TeO_2 rich parts were formed in the center of a focal spot, while zinc migrated to the outside. Alternatively, we assumed that the phase separation occurred in the focal spot. Further investigations are needed to confirm the above mechanism.

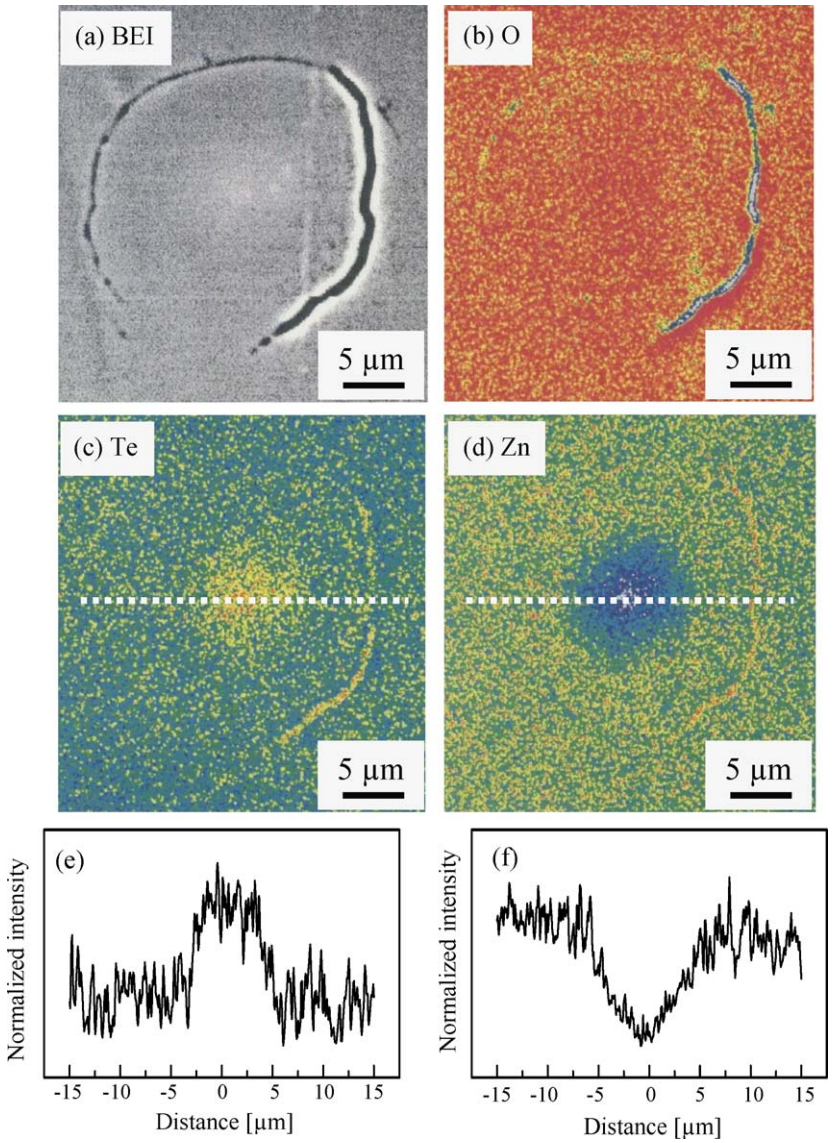

Fig. 7. Backscattering electron image (a) and spectrum mapping images of the elements constituting of the glass sample on the polished surface to the depth of focal spot (b: oxygen, c: tellurium, and d: zinc). Bottom graphs show the line profiles of the intensity of tellurium (e) and zinc (f) on the dotted line in these mapping images.

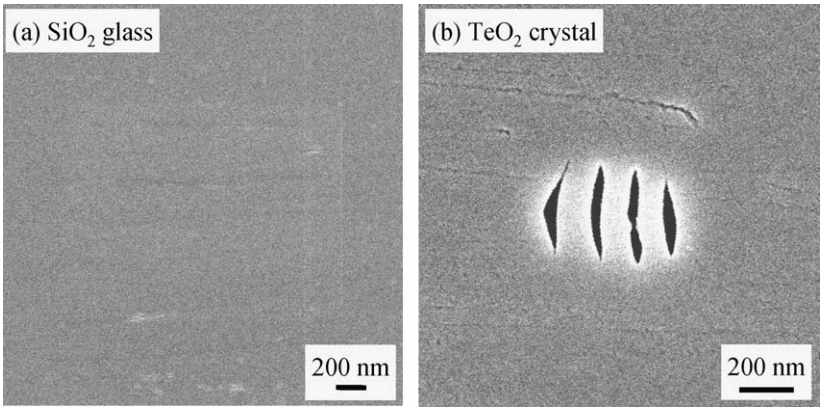

Fig. 8. Secondary electron images of sample surface of fused silica glass (a) and TeO_2 single crystal (b) after polished close to the depth of focal spot [20].

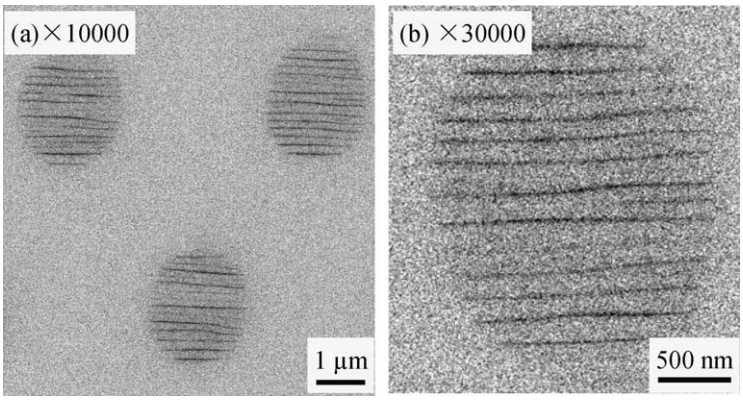

Fig. 9. Backscattering electron images of the polished surface of fused silica glass to the depth of focal spot location. The magnification of (a) and (b) is 10000× and 30000×, respectively [19].

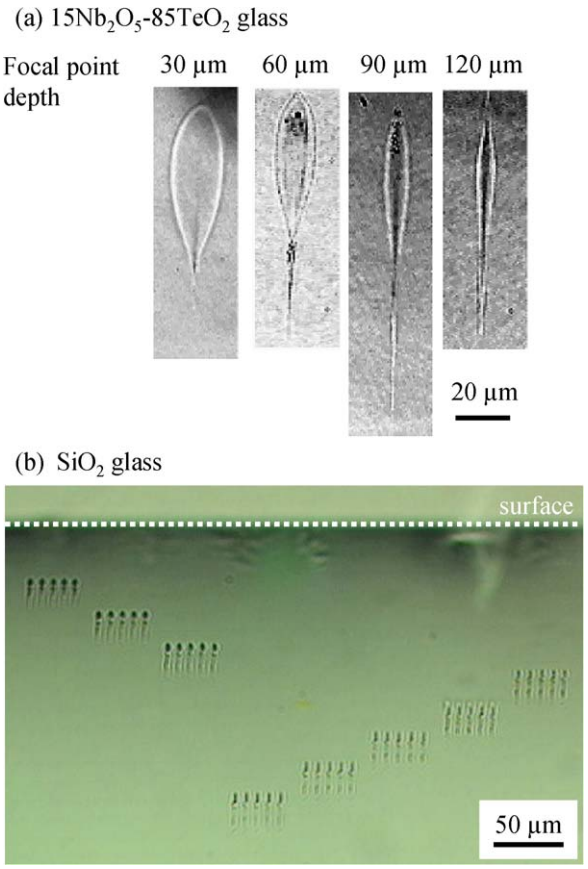

Fig. 10. Optical microscope images (side view) of induced structures inside niobium-tellurite glass and fused silica glass by 1.0 μJ, 120 fs laser pulses at a 200 kHz repetition rate for 1 s. The pulses were focused by a 0.95-NA microscope objective and the focal positions were changed from 20 μm to 200 μm beneath the glass surface. The femtosecond laser was irradiated from above.

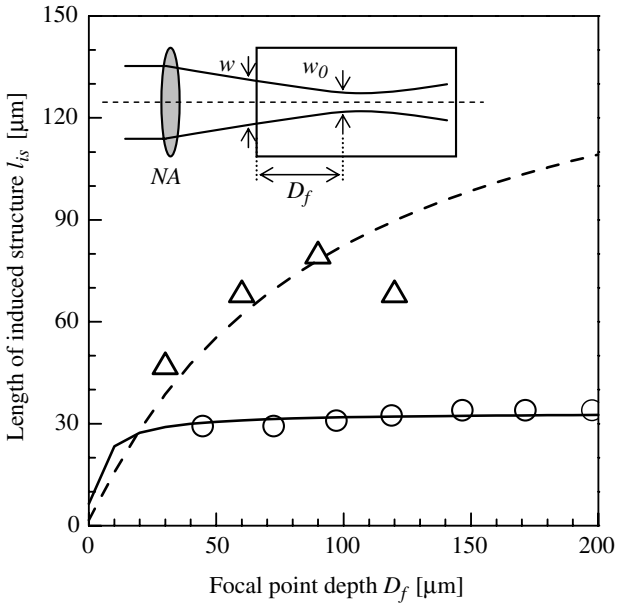

Fig. 11. Dependence of the induced structure after the focused irradiation of 2×10^5 pulses with 1.0 μJ on the various focal point depths. Symbols of (△) and (○) show the experimental data of fused silica glass and niobium-tellurite glass, respectively. Solid and dashed lines show the calculation curves of fused silica glass and niobium-tellurite glass using Eq. (1) (Section 4.4 in text), respectively. Inset shows definition of the parameters w, w_0, and D_f.

4.3. Interference between laser light and electron plasma wave

The following explanation of the polarization-dependent formation of nanostructures is proposed. The light intensity in the focus of the beam is 10^{14} W/cm^2, which is high enough for multiphoton ionization of glass matrix. Once a high free electron density is produced by multiphoton ionization, the material has the properties of a plasma and will absorb the laser energy via one-photon absorption mechanism of inverse Bremstrahlung (Joule) heating. The light absorption in the electron plasma will excite bulk electron acoustic waves. These are longitudinal waves with the electric field component parallel to the direction of propagation. Such an electron plasma wave could couple with the incident light wave only if it propagates in the plane of light polarization. Initial coupling is produced by inhomogeneities induced by electrons moving in the plane of light polarization. The coupling is increased by a periodic

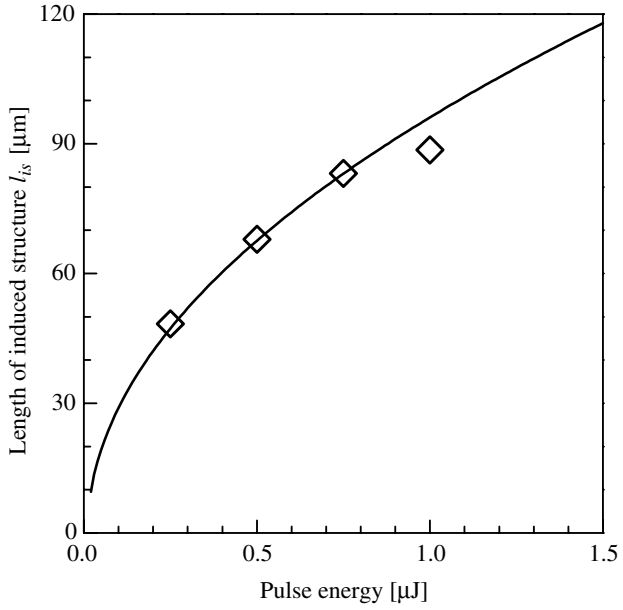

Fig. 12. Dependence of the length of induced structure ~60 μm inside a niobic tellurite glass after the focused irradiation of 2×10^5 pulses for various pulse energies. Symbol of (◇) shows the experimental data and solid line shows the fitting curve using Eq. (3) (Section 4.4 in text).

structure created via a pattern of interference between the incident light field and the electric field of the bulk electron acoustic wave, resulting in the periodic modulation of the electron plasma concentration and the structural changes in glass. Positive feedback will lead to exponential growth of the periodic structures oriented perpendicular to the light polarization, which become frozen within the material. Details of the formation mechanism of the self-organized nanostructures have been described elsewhere [19,20].

4.4. Filamentation-dependent induced structure

Due to the modification of the femtosecond laser propagation by means of the non-linear response of a material, the laser beam induces a refractive-index variation within the material with a larger refractive index at the center of the beam than at its periphery. This self-focusing can occur only if the laser power P is greater than the critical value $P_{cr} = \pi(0.61)^2\lambda_0^2/8n_0n_2$ [31], where λ_0 is the vacuum wavelength of the laser, n_0 is the linear refractive index of a material and the non-linear refractive index n_2 [esu] = $12\pi^2\chi^{(3)}/n_0^2c$ [esu]. Together with the self-focusing effect, the laser beam filamentation occurs only for $P \gg P_{cr}$ due to the balance between self-focusing and self-defocusing arising from plasma formation. Yariv has shown that the characteristic self-focusing depth is given by the formula [32]

$$z_F = \frac{\frac{1}{2}kw^2}{\left(\frac{P}{P_{cr}}-1\right)^{1/2}+\frac{2D_f}{kw_0^2}}, \quad (1)$$

where w_0 is the beam radius at the focal spot, the wave number vector $k = n\omega/c$. The self-focusing depth (z_F), defined as the distance from the entrance surface at which the self-focusing occurs, depends on the critical power for self-focusing and the wave number vector. Furthermore, the beam radius on the entrance surface, w can be expressed by the numerical aperture (NA) of the objective lens and the depth of the focal spot (D_f) (Fig. 11 inset)

$$w = \left(\frac{NA^2}{2}+\frac{1}{2}NA\sqrt{4D_f^2+NA^2}\right)^{1/2}. \quad (2)$$

Besides, Ashkenasi et al. have empirically found that the distance between the entrance surface and the starting point of the bulk modification (modification depth, z_M) is proportional to the self-focusing depth when the picosecond laser pulses were focused on the sample surface [33]. We assumed that the length of induced structure (l_{is}) is proportional to the self-focusing depth because of the ultrahigh peak power density of the femtosecond laser pulses. By comparing the calculated value using Eq. (1) with the experimental results (Fig. 10), we demonstrate the relation between the depth of the focal spot and induced structure (Fig. 11). Table 2 includes linear and non-linear refractive index, the third order susceptibility, the wave number vector inside niobium-tellurite glass and fused silica glass samples. In addition, the ratios of laser power to the critical power for self-focusing (P/P_{cr}) of the pulse energy 1.0 μJ ($P = 8.33$ MW) are also shown. One can see that the ratio of laser power to the critical power for niobium-tellurite glass is about 18 times larger than that of silica glass. The observed variation of the induced structure with the depth of the focal spot is in agreement with the calculation by Eq. (1). For these results, we assumed that the length of the induced structure varies with the depth of the focal spot, because the length is largely dependent on the linear and non-linear refractive index of the material.

Zverev and Pashkov demonstrated that the filamentation length, L_{fil}, generated by self-focusing of the laser radiation in solid dielectrics is expressed as follows [36]:

$$L_{fil} \propto \left[\left(\frac{n_2}{n_0}\right)(P-P_{th})\right]^{1/2}, \quad (3)$$

where P_{th} is the threshold laser power for structural change. If the photoreaction and the filamentation are related to the self-focusing, P_{th} is related to the critical power for self-focusing, P_{cr}. Kondo et al. have observed that the

Table 2
The linear and non-linear refractive index, the third order susceptibility from the literature, wave vector, and the calculated value of the ratio of laser power to the critical power for self-focusing

Glass	SiO_2	$15Nb_2O_5$–$85TeO_2$
n_0	1.45	2.14
n_2 (cm^2/W)	5.26×10^{-16} [34]	6.41×10^{-15} [35]
$\chi^{(3)}$ (esu)	2.80×10^{-14} [34]	7.43×10^{-13} [35]
k (m^{-1})	1.55×10^7	6.74×10^7
P/P_{cr}	6.8	122.2

threshold power for the structural change and the filamentation have the same wavelength-dependence as that of P_{cr} [37]. We fitted the experimental results with using P_{cr} in place of P_{th} in Eq. (3), assuming the filamentation length is proportional to the length of induced structure (Fig. 12). We confirmed that the length of the induced structure depends on the pulse energy. On the other hand, the formation of high-density electron plasma resulting from the interactions between femtosecond pulses and materials causes a decrease in the real part of the refractive index, and then acts as a concave lens [38]. The refractive-index variation due to the plasma formation could compensate for the self-focusing due to the optical Kerr effect. After the laser pulse has passed, the electron plasma is rapidly quenched. It is necessary to clarify the mechanism of the structural changes along the laser propagation axis from the viewpoint of the electron plasma formation.

5. Conclusion

We have demonstrated the shape control of an induced structure in the bulk of Ag^{+}-doped silicate glass, fused silica glass, and tellurite glass by tightly focused femtosecond laser irradiation. Due to the aggregation of Ag nanoparticles at the depth of the focal point, rugby-ball-like asymmetric induced structures were observed inside Ag^{+}-doped silicate glass. By comparing different thermal diffusivity materials, we found that there is a relation between the size of the induced structure and the time interval between successive femtosecond laser pulses. In the case of zinc-tellurite glass, TeO_2 rich parts were formed in the center of a focal spot, while zinc migrated to the outside. Moreover, we observed the length of an induced structure varies with the depth of the focal spot location from sample surface. The length of the induced structure depends on the pulse energy of the femtosecond laser irradiation. Furthermore, we observed the emergence of self-organized periodic structure of nanometer size inside fused silica glass and tellurium dioxide single crystal after irradiation by intense femtosecond laser single beam. The phenomenon is interpreted in terms of interference between the incident light field and the electric field of bulk electron plasma wave, resulting in periodic modulation of electron plasma concentration and permanent structural changes in glass. The observed phenomena are useful in the fabrication of the three-dimensional symmetric micro and nanostructures for many monolithic photonic devices and microelectromechanical system applications.

Acknowledgments

This work was partially supported by Japanese Ministry of Education, Culture, Sports, Science and Technology (MEXT), and by the Mitsubishi Foundation. They are the computational materials science unit in Kyoto University, the Grant-in-Aid for Scientific Research on Priority Areas (No. 751), (B), and the 21st century COE program.

References

[1] B.N. Chickov, C. Momma, S. Nolte, F.V. Alvensleben, A. Tunnermann, Appl. Phys. A 63 (1996) 109.
[2] E.N. Glezer, M. Milosavljevic, L. Huang, R.J. Finlay, T.-H. Her, J.P. Callan, E. Mazur, Opt. Lett. 21 (1996) 2023.
[3] J. Qiu, K. Miura, K. Hirao, Jpn. J. Appl. Phys. 37 (1998) 2263.
[4] J. Qiu, K. Miura, H. Inouye, Y. Kondo, T. Mutsuyu, K. Hirao, Appl. Phys. Lett. 73 (1998) 1763.
[5] Y. Kondo, T. Suzuki, H. Inouye, K. Miura, T. Mitsuyu, K. Hirao, Jpn. J. Appl. Phys. 37 (1998) L94.
[6] M. Will, S. Nolte, B.N. Chichkov, A. Tunnermann, Appl. Opt. 41 (2002) 4360.
[7] D.N. Fittinghoff, C.B. Schaffer, E. Mazur, J.A. Squier, IEEE J. Sel. Top. Quantum Electron. 7 (2001) 559.
[8] K. Minoshima, A.M. Kowalevicz, I. Hartl, E.P. Ippen, J.G. Fujimoto, Opt. Lett. 26 (2001) 1516.
[9] Y. Sikorski, A.A. Said, P. Bado, R. Maynard, C. Florea, K.A. Winick, Electron. Lett. 36 (2000) 226.
[10] K. Miura, J. Qiu, T. Mitsuyu, K. Hirao, Nucl. Instr. Methods Phys. Res. B 141 (1998) 726.
[11] Y. Kondo, K. Nouchi, T. Mitsuyu, M. Watanabe, P.G. Kazansky, K. Hirao, Opt. Lett. 24 (1999) 646.
[12] B.H. Cumpston, S.P. Ananthavel, S. Barlow, D.L. Dyer, J.E. Ehrlich, L.L. Erskine, A.A. Heikal, S.M. Kuebler, I.-Y.S. Lee, D. Mccord-Naughton, J. Qin, H. Rökel, M. Rumi, X.-L. Wu, S.R. Marder, J.W. Perry, Nature 398 (1999) 51.
[13] H.B. Sun, Y. Xu, S. Joudkazis, K. Sun, M. Watanabe, J. Nishii, S. Matsuo, H. Misawa, Opt. Lett. 26 (2001) 325.
[14] B.C. Stuart, M.D. Feit, S. Herman, A.M. Rubenchik, B.W. Shore, M.D. Perry, Phys. Rev. B 53 (1996) 1749.
[15] M. Lenzner, L.J. Kruger, S. Sartania, Z. Cheng, C. Spielmann, L.G. Mourou, W. Kautek, F. Krausz, Phys. Rev. Lett. 80 (1998) 4076.
[16] P.G. Kazansky, E. Bricchi, C. Corbari, B. Klappauf, O. Deparis, J. Qiu, Y. Shimotsuma, K. Hirao, Proc. SPIE Int. Soc. Opt. Eng. 5399 (2003) 13.
[17] C.B. Schaffer, A. Brodeur, E. Mazur, Meas. Sci. Technol. 12 (2001) 1784.
[18] P.G. Kazansky, H. Inoue, T. Mitsuyu, K. Miura, J. Qiu, K. Hirao, F. Starrost, Phys. Rev. Lett. 82 (1999) 2199.
[19] Y. Shimotsuma, P.G. Kazansky, J. Qiu, K. Hirao, Phys. Rev. Lett. 91 (2003) 247405.
[20] Y. Shimotsuma, J. Qiu, P.G. Kazansky, K. Hirao, Mod. Phys. Lett. B 19 (2005) 225.
[21] M.R. Kasaai, V. Kacham, F. Theberge, S.L. Chin, J. Non-Cryst. Solids 319 (2003) 129.
[22] A. Ben-Yakar, R.L. Byer, A. Harkin, J. Ashmore, H.A. Stone, M. Shen, E. Mazur, Appl. Phys. Lett. 83 (2003) 3030.
[23] B.C. Stuart, M.D. Feit, A.M. Rubenchik, B.W. Shore, M.D. Perry, Phys. Rev. Lett. 74 (1995) 2248.
[24] L. Sudrie, A. Couairon, M. Franco, B. Lamouroux, B. Prade, S. Tzortzakis, A. Mysyrowicz, Phys. Rev. Lett. 89 (2002) 186601.
[25] J. Qiu, M. Shirai, T. Nakaya, J. Si, X. Jiang, C. Zhu, K. Hirao, Appl. Phys. Lett. 81 (2002) 3040.
[26] H. Zeng, J. Qiu, X. Jiang, C. Zhu, F. Gan, J. Phys.: Condens. Matter 16 (2004) 2901.
[27] Q. Zhao, J. Qiu, X. Jiang, C. Zhao, C. Zhu, Opt. Exp. 12 (2004) 4035.
[28] C.B. Schaffer, A. Brodeur, J.F. Garcia, E. Mazur, Opt. Lett. 26 (2001) 93.
[29] J. Qiu, P.G. Kazansky, J. Si, K. Miura, T. Mitsuyu, K. Hirao, A.L. Gaeta, Appl. Phys. Lett. 77 (2000) 1940.
[30] A. Nukui, T. Taniguchi, M. Miyata, J. Non-Cryst. Solids 293–295 (2001) 255.
[31] R.W. Boyd, Nonlinear Optics, 2nd Ed., Academic, Boston, 2002.
[32] A. Yariv, Quantum Electronics, Wiley, New York, 1975.
[33] D. Ashkenasi, H. Varel, A. Rosenfeld, S. Henz, J. Herrmann, E.E.B. Cambell, Appl. Phys. Lett. 72 (1998) 1442.

[34] H. Nasu, T. Uchigaki, K. Kamiya, H. Kanbara, K. Kubodera, Jpn. J. Appl. Phys. 31 (1992) 3899.
[35] L. Canioni, M.-O. Martin, B. Bousquet, L. Sarger, Opt. Commun. 151 (1998) 241.
[36] G.M. Zverev, V.A. Pashkov, Sov. Phys. JETP 30 (1970) 616.
[37] Y. Kondo, K. Miura, T. Suzuki, H. Inoue, T. Mitsuyu, K. Hirao, J. Non-Cryst. Solids 253 (1999) 143.
[38] N. Bloembergen, IEEE J. Quantum Electron. QE-10 (1974) 375.